Biosensors and Bioelectronics: X 18 (2024) 100476

Contents lists available at ScienceDirect

Biosensors and Bioelectronics: X

journal homepage: www.journals.elsevier.com/biosensors-and-bioelectronics-x

Wearable sensor for real-time monitoring of oxidative stress in simulated exhaled breath

M.G. Bruno [a], B. Patella [a], M. Ferraro [b], S. Di Vincenzo [b], P. Pinto [b,c], C. Torino [d], A. Vilasi [d], M.R. Giuffrè [e], V.B. Juska [f], A. O'Riordan [f], R. Inguanta [a,b,*], C. Cipollina [e,b], E. Pace [b], G. Aiello [a]

[a] Dipartimento di Ingegneria, Università degli Studi di Palermo, Viale delle Scienze, 90128 Palermo, Italy
[b] Institute of Translational Pharmacology, National Research Council, 90146 Palermo, Italy
[c] Department of Public Health, Experimental and Forensic Medicine, University of Pavia, Pavia, 27100, Italy
[d] Institute of Clinical Physiology, National Research Council, 89124 Reggio Calabria, Italy
[e] Ri.MED Foundation, 90133 Palermo, Italy
[f] Nanotechnology Group, Tyndall National Institute, University College Cork, Cork, T12 R5CP, Ireland

ARTICLE INFO

Keywords:
Electrochemical sensors
Human bronchial epithelial cells
Oxidative stress
Real-time monitoring
Workers' health and safety
Wearable sensors

ABSTRACT

High concentrations of H_2O_2, indicative of increased oxidative stress in the lung, are observed in the exhaled breath of individuals affected by different respiratory diseases. Therefore, measuring H_2O_2 in exhaled breath represents a promising and non-invasive approach for monitoring the onset and progression of these diseases. Herein, we have developed an innovative, inexpensive, and easy-to-use device for the measurement of H_2O_2 in exhaled breath. The device is based on a silver layer covered with an electrodeposited thin film of chitosan, that ensures the wettability of the sensor in a humid atmosphere. The s-ensor was calibrated in the aerosol phase using both phosphate buffer solution and cell culture medium. In the buffer, a sensitivity of 0.110 ± 0.0042 μA μM^{-1} cm^{-2} (RSD: 4%) and a limit of detection of 30 μM were calculated, while in the cell culture medium, a sensitivity of 0.098 ± 0.0022 μA μM^{-1} cm^{-2} (RSD 2%) and a limit of detection of 40 μM were obtained. High selectivity to different interfering species was also verified. The sensor was further tested versus an aerosol phase obtained by nebulizing the culture medium derived from human bronchial epithelial cells that had been exposed to pro-oxidant and antioxidant treatments. The results were comparable with those obtained using the conventional cytofluorimetric method. Finally, sensor was tested in real exhaled breath samples and even after undergoing physical deformations. Data herein presented support that in future applications this device can be integrated into face masks allowing for easy breath monitoring.

1. Introduction

Asthma, chronic obstructive pulmonary disease (COPD) and occupational lung diseases are the most common chronic respiratory diseases in the world (Anh et al., 2005; Shukla et al., 2020), with tobacco smoke, air pollution, exposure to chemicals and dusts, frequently present in industrial work environments, representing the major risk factors. The World Health Organization (WHO) has recently launched a Chronic Respiratory Diseases Programme to support the Member States in their efforts to reduce occupational risks through continuous monitoring of workers' health status ("https://www.who.int/health-topics/chronic-respiratory-diseases#tab=tab_1," n.d.) in addition to adopting protective equipment (masks) ("https://www.who.int/europe/health-topics/chronic-respiratory-diseases#tab=tab_1," n.d.). Such monitoring can be performed by analyzing easily accessible body fluids including urine, sweat, tears, and breath (Lin et al., 2022). Among these, breath is a very interesting biofluid as it contains relevant information concerning the respiratory health status of an individual (Kaloumenou et al., 2022). The aerosol phase of exhaled breath (EB) consists of aqueous droplets dispersed in a gaseous phase (Davis, 2020; Pleil et al., 2018). EB contains more than 200 compounds (Das and Pal, 2020), including volatile organic compounds (VOCs), hydrogen peroxide (H_2O_2), ammonia and nitric oxide (Boots et al., 2012). The analysis of H_2O_2 in EB is considered a promising, non-invasive approach for supporting early diagnosis and monitoring of respiratory diseases (Das and Pal, 2020). The concentration of H_2O_2 in Exhaled Breath Condensate

* Corresponding author. Dipartimento di Ingegneria, Università degli Studi di Palermo, Viale delle Scienze, 90128 Palermo, Italy.
E-mail address: rosalinda.inguanta@unipa.it (R. Inguanta).

https://doi.org/10.1016/j.biosx.2024.100476
Received 25 November 2023; Received in revised form 12 March 2024; Accepted 31 March 2024
Available online 6 April 2024

(EBC) samples varies over time and ranges from 0.02 up to 8 μM (Dekhuijzen et al., 1996; Inonu et al., 2012; Murata et al., 2014; Nagaraja et al., 2012; Rysz et al., 2007), depending on health conditions.

The conventional method for EB analysis is the collection of EBC (Grob et al., 2008). This sampling procedure requires specialized laboratories and it is therefore inadequate for real-time diagnostics (Połomska et al., 2021). The urgent need and interest to monitor respiratory pathologies has driven the development of innovative technologies (Szunerits et al., 2023; Tiele et al., 2020), and low-cost and open-source solutions that allow for real-time and in situ monitoring of breath biomarkers (Ainla et al., 2018; Aznar-Poveda et al., 2018; Lu et al., 2023). Electrochemical sensors are simple to use, may be miniaturised, require small sample volumes (μl) and very small and portable instrumentation (O'Sullivan et al., 2022). This technology is thus considered a key enabler of more efficient and inclusive healthcare services performed "near the patient" by non-professional personnel, consistent with modern approaches to personalized medicine.

Many papers have reported electrochemical sensors immersed in EBC (Bhide et al., 2022; Diouf et al., 2020). However, the direct application of these devices for EB monitoring is still limited due to the difficulty of undertaking analysis in the absence of a liquid electrolyte. This shortcoming may be addressed by employing absorbent materials capable of trapping the EB such as paper or biopolymers, on an electrode surface (Lopresti et al., 2022). Absorbent materials can be humidified, thus allowing electrolytic contact with the underlying electrodes. To the best of our knowledge, very few papers can be found in the literature using this approach. In particular, Maier et al. have used a paper-based screen-printed electrode for the quantification of H_2O_2 in the linear range of 40–320 μM with a sensitivity of 0.002 μA μM^{-1} cm^{-2}. A very similar approach was proposed by Fiore et al. who obtained a paper-based sensor capable of detecting H_2O_2 in the range from 0.3 to 2.3 M (Fiore et al., 2021). In both papers, Prussian blue (PB) was used to increase the sensor sensitivity. However, the use of PB has some drawbacks, due to its high instability and short lifetime (Manabe et al., 2020; Wang et al., 2014). The results obtained by Maier et al. and Fiore et al. are very interesting because the availability of smart face masks, simultaneously ensuring EB collection and analysis, will have an increasing socio-economic impact. They represent a convenient and cost-effective solution for non-invasive direct monitoring of individuals with respiratory diseases (Szunerits et al., 2023).

Herein, we propose a silver/chitosan sensor for the quantification of H_2O_2 in the aerosol phase. Chitosan was selected because of its biocompatibility, biodegradability and very high swelling degree (Khalid et al., 2002). The sensor comprised three electrodes fabricated using the silver layer from recycled optical storage disks, as described previously (Lopresti et al., 2022; Patella et al., 2022a). The sensor was characterized using physical and chemical analyses and employed to quantify H_2O_2 both in the liquid and the aerosol phase. Importantly, the ability of the sensor to quantify H_2O_2 released by human bronchial epithelial cells, 16HBE, was tested. 16HBE cells were exposed to cigarette smoke extract (CSE, an inducer of oxidative stress), in the presence/absence of the antioxidant N-acetylcysteine (NAC) and the drug formoterol (FORM). The conditioned medium was nebulized to mimic exhaled breath and H_2O_2 concentration in the aerosol phase was measured. Finally, the sensor was also tested using real samples of EBC.

2. Experimental

The details of experimental methods are presented in the Supplementary Materials. Briefly, the sensor was fabricated by peeling off the silver layer from compact discs (CDs) using double tape, as described previously (Lopresti et al., 2022; Patella et al., 2022a). A three electrodes configuration (Fig. S1, see Scheme S1) was produced using a laser cutter. An Ag/AgCl paste was applied to the reference area to produce a pseudo-reference electrode (RE). A graphite paste was then used to coat the counter electrode area to obtain a stable counter electrode (CE). The Ag working electrode (WE) was not modified. A chitosan layer was electrodeposited on top of all three electrodes to allow contact between electrodes and electrolyte.

Field Emission Scanning Electron Microscopy (FESEM), Energy Dispersive Spectroscopy (EDS), X-ray diffraction (XRD), Raman spectroscopy, FT-IR analysis and contact angle measurements were used to characterize the sensor.

Sensor performance was evaluated using Linear Sweep Voltammetry (LSV). Tests were carried out in the liquid phase (phosphate buffer solution, PBS) and, to simulate the humid atmosphere of EB, were also repeated by nebulizing solutions with different concentrations of hydrogen peroxide. The selectivity of the sensor was also verified for common interfering species. Finally, the sensor was also used both analyse the cell culture medium of 16HBE cells (MEM) and real samples of EBC.

A cell line of immortalized human normal bronchial epithelial, 16HBE, was pre-treated with NAC (1 mM) for 2 h, with FORM (10-8 M) for 30 min and then exposed to CSE 20% for 24 h. CSE was prepared by burning two cigarettes (3R4F -Kentucky - The Tobacco Research Institute, University of Kentucky), without any filter, in 20 mL of PBS using a Watson-Marlow 323 E/D peristaltic pump. The solution was filter-sterilized using a 0.22 μm pore filter and was assumed to be 100% CSE. Following stimulation, the culture medium was collected to measure the H_2O_2 using the sensor, and cells were harvested to evaluate intracellular oxidative stress by flow cytometry using the Mito-SOX™ Red probe.

3. Results and discussions

3.1. Electrode fabrication and characterization

The electrodeposition of the chitosan layer was carefully optimized to obtain a thin, homogeneous, and uniform film covering the entire sensor surface. This layer permitted absorption of the EB, allowing any H_2O_2 present in the sample to diffuse toward the surface of a WE where it could be detected.

The electrodeposition of chitosan occurred as follows (Avcu et al., 2019):

$$\text{Chit-NH}_2 + \text{H}_3\text{O}^+ \rightarrow \text{Chit-NH}_3^+ + \text{H}_2\text{O} \quad \text{(I)}$$

$$2\text{H}_2\text{O} + 2\text{e}^- \rightarrow \text{H}_2 + 2\text{OH}^- \quad \text{(II)}$$

$$\text{O}_2 + 2\text{H}_2\text{O} + 4\text{e}^- \rightarrow 4\text{OH}^- \quad \text{(III)}$$

$$\text{Chit-NH}_3^+ + \text{OH}^- \rightarrow \text{Chit-NH}_2 + \text{H}_2\text{O} \quad \text{(IV)}$$

As a result of reaction (I), conducted at low pH, the protonation of amine groups of chitosan occurred. These positively charged chitosan molecules moved toward the cathode surface. Following reactions (II) and (III), the well-known electrogeneration of base reactions (Nobial et al., 2007), the local pH at a cathode surface increased. When an interfacial pH value of about 6.5 was reached (corresponding to the pKa of chitosan (Khalid et al., 2002)), the chitosan macromolecules, according to reaction (IV), formed an insoluble deposit on an electrode surface. The electrodeposition of chitosan was optimized in terms of solution concentrations (1–5 g/L), deposition time (1800–3600 s), and applied potential (5–10 V). More compact and uniform chitosan films were obtained at higher concentrations and higher applied potentials. For deposition carried out at longer deposition times, a thicker film was obtained, which caused a reduction in the sensitivity of the sensor (Besra and Liu, 2007). Thus, the optimized conditions for chitosan deposition were identified as 5 g/L, at an applied potential of 10 V, for 1800 s.

Following fabrication, sensor was characterized using different physical-chemical tests. The EDS spectrum (Fig. S3c) shows the presence of C and O confirming the deposition of chitosan. The other elements were attributed to the CD-peeled layer (Fig. S2b) (Patella et al., 2022a).

EDS analyses were performed in different areas of the electrodes to confirm the uniformity of deposition. The typical morphology of chitosan films formed by electrodeposition (Kowalski et al., 2015) can be observed in the SEM images presented in Fig. 1. In Fig. 1a, an extremely wrinkled sponge-like morphology, apparently made up of pores of various sizes, can be observed. This morphology is due to the entrapment of the hydrogen gas formed by the reaction (II) (Altomare et al., 2012). The chitosan film can be detected in the entire sensor area, Fig. 1b. The deposition of chitosan on the surface between CE and WE also occurred, which is highly critical to ensure the electrolytic contact between the three electrodes. To further understand the internal morphology of the chitosan, a layer was peeled off from a WE and a cross-section analysis was performed. Fig. 1c (Fig. S3 a and b), shows a SEM image of the cross-sectional view and demonstrates the multi-layered structure of the chitosan. From these images, the thickness of the chitosan layer was measured. Thickness measurement was made on different parts of the same sample and also on different samples. In all cases, the thickness ranged between 10 μm and 40 μm. The cross-section images clearly show that the pores on the surface are actually a thinner area of chitosan. The optical images before and after the swelling in PBS show that this process tends to cancel the surface roughness of the film with the formation of a uniform gel layer (Fig. S4).

The wettability of a sensor surface (with and without the chitosan film) was studied by measuring the contact angle which is known to decrease with increased surface hydrophilicity. The contact angle was measured using PBS as the wetting liquid. As shown in Fig. 1d, the value of the contact angles changed from ~89 ± 3.7°, for the CD-peeled layer, to ~52 ± 4.5°, for the CD-peeled layer covered with chitosan and dried in the air. As expected, this value decreased further to ~5 ± 2.3°, when the chitosan film was swelled in PBS (Khalid et al., 2002). The Ag layer present in the CD, due to its rough morphology, was practically hydrophobic and therefore had the highest contact angle. The very low value measured in the case of the swelled film indicated that the presence of chitosan allowed a fast and efficient wetting of the entire sensor surface (Wang et al., 2023). This result is very important because it guarantees the correct operation of the sensor within an aerosol phase.

The CD-peeled Ag layer before and after the deposition of chitosan film was also studied by X-ray diffraction (Fig. S5). The diffraction peaks of silver and chitosan were identified through comparisons with the available database (card number 39-1894 for chitosan and 04-0783 for silver) (Lafuente et al., 2015). In the pattern of the CD-peeled layer before chitosan deposition, the diffraction peaks at ~38.3° and 44.5°, corresponding to (111) and (200) plans of the face-centered cube structure of Ag, were identified. The other peaks came from the substrate of the peeled layer of CD (Patella et al., 2022a). After chitosan deposition (black pattern), the broad and low-intensity peaks at ~9.6° and 19.8° appeared and were attributed to the diffraction plans (020) and (110) of semicrystalline chitosan (Jiang et al., 2010). The presence of the chitosan shielded the peaks coming from the CD-peeled layer. This was expected because, in a multilayer system, the intensity of the diffraction peaks coming from the internal layers is always lower than the intensity of the peaks relating to the layers closest to the surface.

The sensor was also characterized by micro-Raman spectroscopy and FT-IR analysis which was performed in different areas of a sensor to verify the presence of different materials (Scheme S1). Raman spectra were collected in CE, WE, and RE areas (Fig. 2a). In the CE spectrum (CD-peeled layer/graphite paste/chitosan layer) all Raman modes were attributable to graphite (Ferrari, 2007). In particular, both the first-order (1328 cm^{-1} (D1 band) and 1577 cm^{-1} (G band)) and the second-order (2685 cm^{-1} (2D band)) Raman bands were present. Also, the weak defect-induced bands at 2437 cm^{-1} (G* band) and at 2942 cm^{-1} (D + G band) with a very low intensity were present (Kaniyoor and Ramaprabhu, 2012). The fluorescence emission was due to the polymer layer. From the working electrode (CD-peeled layer/chitosan layer), despite the strong background fluorescence emission (Han et al., 2020), numerous characteristic Raman modes of chitosan (Table S1) (Ren et al.,

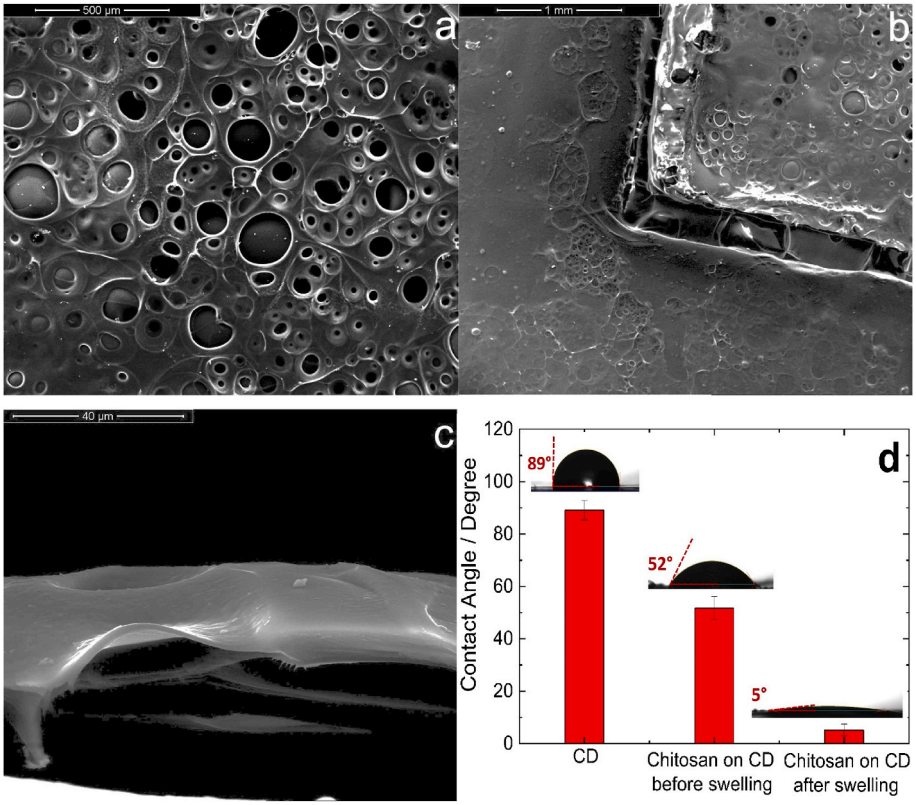

Fig. 1. Chitosan layer before swelling: a) SEM image of WE area; b) SEM image of the area between CE and WE. c) Tilted cross-sectional view of chitosan layer peeled from a WE d) Mean values of contact angle measured on CD-peeled layer before and after chitosan deposition and before and after chitosan swelling.

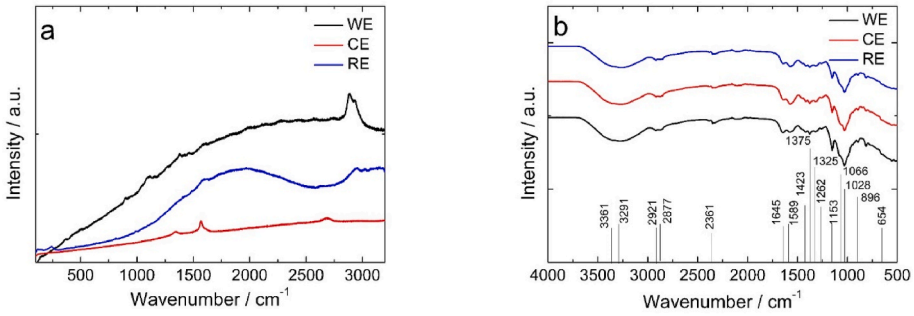

Fig. 2. a) Raman and b) FT-IR spectra collected in the different areas of the sensor after the chitosan electrodeposition.

2014) were identified. This analysis provided further evidence of the presence of the chitosan. The Raman bands of chitosan were not present in the CE area because they were shielded by the bands of graphite. In the spectrum of the reference electrode (CD-peeled layer/Ag–AgCl paste/chitosan layer), several Raman bands of chitosan (with a very low intensity due to fluorescence signal) were identified. AgCl was also identified by the modes at about 145 and 237 cm^{-1}. Also, in the FT-IR spectra, the characteristic peaks of chitosan film deposited on the surface of the sensor were identified (Fig. 2b). The strong band between 3361 and 3291 cm^{-1} corresponds to N–H and O–H stretching, while the bands at 2921 and 2877 cm^{-1} are assigned to the asymmetric and symmetric C–H stretching vibration. The bands at around 1645 cm^{-1} and 1325 cm^{-1} were characteristic of C═O stretching of amide I and C–N stretching of amide III, respectively. The band at 1589 cm^{-1} was attributed to the N–H bending of the primary amine. The bands at 1423 and 1375 cm^{-1} confirm the CH_2 bending and CH_3 symmetrical deformations, while the band at 1153 cm^{-1} was associated with asymmetric stretching of the C–O–C bridge. The signals at 1066 and 1028 cm^{-1} can be attributed to C–O stretching, the bands at 1260 cm^{-1}, 896 cm^{-1} and 654 cm^{-1} correspond to the –OH bending vibration, and to the –CH out-of-plane vibration and the –NH twist vibration, respectively (Jiang et al., 2010). These peaks were obtained from the regions of each electrode on the sensor confirming the full coverage of the chitosan layer all over the sensor surface.

3.2. Electrochemical characterization

The electrochemical behavior of H_2O_2 using fabricated sensor was studied by CVs performed at different scan rates, in a solution of PBS containing 5 mM of H_2O_2. Fig. 3a shows that, with the increase of scan rate, the reduction peaks moved toward more cathodic potentials. The corresponding oxidation peaks were absent, confirming that the process is irreversible (Cai et al., 2018a). In Fig. 3b, it can be observed that the reduction peak current density was proportional to the square root of the scan rate ($R^2 = 0.9987$). This result is indicative of a diffusion-controlled process, in agreement with the data obtained in (Cai et al., 2018a).

Sensor performance was analyzed using LSV and all LSV curves are reported following baseline subtraction. LSV was performed in both liquid solutions and in the aerosol phase for comparison. In liquid solution, LSV was carried out in the potential range from 0.1 to −1 V vs Ag/AgCl using PBS as blank (Fig. S6). In the investigated range, the presence of two peaks was observed. The first at ~0 V is independent of increasing concentrations of H_2O_2 in the solution, while the second at about −0.6 V, increases with the concentration of H_2O_2. The first peak is due to the reduction of dissolved oxygen to H_2O_2, following the reaction (V) (Jiang et al., 2019):

$$O_2 + 2H_2O + 2e^- \rightarrow H_2O_2 + 2OH^- \quad (V)$$

The peak present at about −0.6 V is related to the reduction of H_2O_2 to water, following the reaction (VI) (Tran et al., 2018):

$$H_2O_2 + 2H^+ + 2e^- \rightarrow 2H_2O \quad (VI)$$

The intensity of the peak at ~0.6 V (Fig. S6a) increases linearly with H_2O_2 concentration in the range from 100 μM to 500 μM. The shift in the potential peak of the H_2O_2 reduction agrees with Nernst's equation (Cai et al., 2018b). From the calibration line (Fig. S6b), a sensitivity of 0.062 ± 0.0024 μA μM^{-1} cm^{-2} (R^2 = 0.9996) was obtained. A limit of detection (LOD) of 60 μM was calculated using the following equation:

$$LOD = 3.3\,\frac{SD}{S}$$

where SD is the standard deviation of the blank response (obtained by measuring 10 times the current density of the blank) and S is the sensitivity of the sensor.

LSV tests were performed by exposing the electrode to nebulized solutions to simulate the humid atmosphere of EB. First, the sensor was immersed in PBS solution to swell the chitosan layers. Following this, the LSV curves were recorded after 10 s of nebulization to allow impregnation of a sensor homogeneously with the nebulized solutions. Importantly, using this approach, the pre-immersion of a sensor in PBS to swell the chitosan could be avoided. One-minute duration of nebulization allowed the stabilization of the sensor without the initial PBS treatment. In Fig. 4 the LSV curves in nebulized solutions (Fig. 4a) and

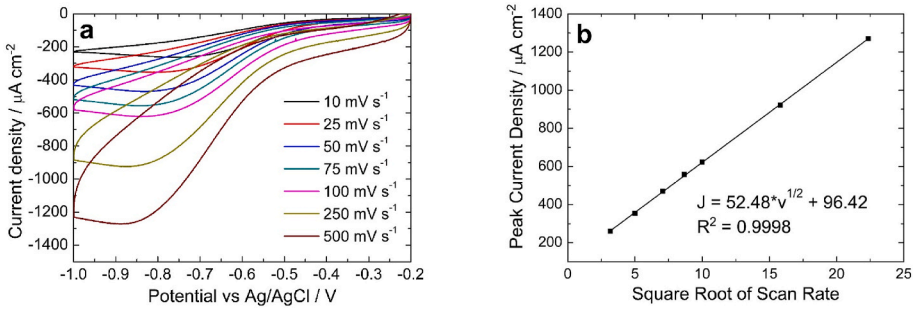

Fig. 3. a) CVs performed in the potential range from −0.2 V to -1 V vs Ag/AgCl in PBS containing H_2O_2 5 mM. b) Effect of scan rate on peak current density.

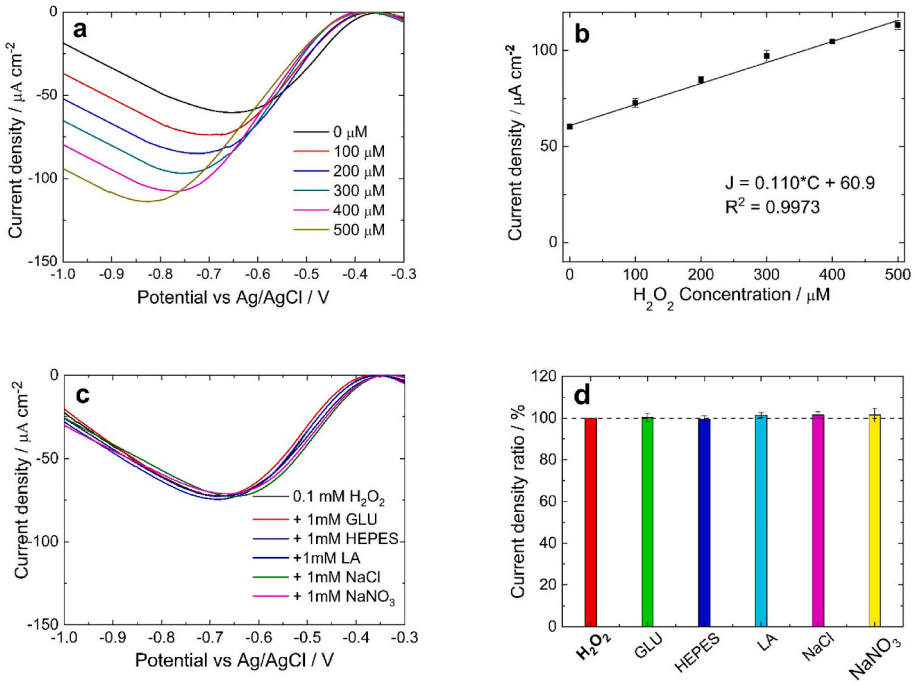

Fig. 4. a) LSV tests in nebulized solutions at different concentrations of H_2O_2. b) Corresponding calibration line with SD error bars (N = 3). c) LSV tests in PBS solution containing 0.1 mM of H_2O_2 and 1 mM of interfering species. d) Effect of interfering species on the H_2O_2 detection. (GLU: glucose; LA: Lactic Acid).

the relative calibration line (Fig. 4b) are reported. From these experiments, a sensitivity of 0.110 ± 0.0042 μA μM^{-1} cm^{-2} ($R^2 = 0.9973$) and a LOD of 30 μM were calculated with a linear range from 100 μM to 500 μM. This sensitivity is higher compared to current literature data concerning the quantification of hydrogen peroxide in an aerosol phase (Fiore et al., 2021; Maier et al., 2019; Toniolo et al., 2001) (Table S2). The mean relative standard deviation (RSD) of each experiment was 3.8% for liquid solutions and 4% for aerosol solutions. These low RSD values indicate that the applied fabrication protocol was reproducible. Of note, sensor displayed a higher sensitivity when used to detect hydrogen peroxide in nebulized solutions compared to liquid solutions. This result agrees with the data obtained by Fiore et al. (2021). The higher sensitivity for the aerosol phase compared to the liquid is attributable to the presence of the chitosan absorbent layer that leads to the phenomenon of pre-concentration of the analyte. In particular, when the absorbent layer is exposed to the aerosol phase, it tends to dry quickly due to the evaporation of the water. Following this phenomenon, the analyte becomes concentrated, leading to higher sensitivity. To confirm this phenomenon, H_2O_2 was measured after different nebulizing times. To perform these tests, a solution containing the same concentration of H_2O_2 was nebulized and LSV started after 10, 30, 60 and 120 s. Results show that after 60s of nebulization, the H_2O_2 detected from the sensor was about two times higher than the value measured after 10s (Fig. S7). The nebulization time cannot be increased infinitely, because, due to its thickness, the chitosan film tends to saturate quite quickly, as demonstrated by the trend of the curve in Fig. S7. Thus, the sensitivity of a sensor can be increased by adjusting the nebulization time and by further optimizing the thickness of the chitosan film. In the case of the sensor immersed in a liquid phase, this phenomenon obviously cannot occur due to short analysis times.

The performance of a sensor in complex matrices was also investigated. Sensor was used to quantify H_2O_2 present in a nebulized conditioned medium of 16HBE cells. Before proceeding with the measurement, sensor performance was studied in the presence of different interfering species (glucose, HEPES, lactic acid, sodium chloride, sodium nitrate) that could be found in culture media or that could be generated by cells (Arodin Selenius et al., 2019; Baker et al., 2009). 1 mM of interfering species was added to the nebulized solution containing 0.1 mM of H_2O_2. The results are shown in Fig. 4c as LSV curves and in Fig. 4d as the ratio between the peak current for H_2O_2 reduction measured in the presence and in the absence of each interfering species. Although the concentration of interfering species was 10 times higher than the concentration of H_2O_2, a negligible effect was observed in terms of both peak current density and peak potential confirming that the sensor has a high selectivity towards H_2O_2 and can discriminate H_2O_2 response from the different interferents.

A dedicated calibration line was then constructed using the culture medium of 16HBE, MEM, as a blank. This was required to take into account the complexity of MEM and possible interference of MEM matrix with sensor performance (Patella et al., 2022b). Therefore, MEM containing different amounts of H_2O_2 was nebulized and LSVs were performed (Fig. 5a). From the calibration line reported in Fig. 5b a sensitivity of 0.098 ± 0.0022 μA μM^{-1} cm^{-2} ($R^2 = 0.9958$) was obtained with a mean RSD of about 2% and a LOD of 40 μM. These values are very close to those obtained in nebulized PBS, strongly suggesting that sensor performance remains unchanged in MEM culture medium and that sensor can work in a very complex matrix.

Table 1 reassumes the features of the sensor tested in the different conditions. In each working condition, the sensor repeatability was evaluated by calibrating the same sensor three times.

The flexibility of the sensor was also investigated, by testing its performances after several and different physical deformation cycles. The Sensors was deformed by bending and twisting (Fig. S8) five times and then used for the detection of H_2O_2 in the aerosol phase. The bent and twisted electrodes demonstrated the same behavior as pristine sensor, and thus indicating that these deformations did not alter their functionality (Fig. S9). These tests strongly support the compatibility of this sensor for use in a face mask without loss of performance.

Measurement of H_2O_2 in the aerosol phase of nebulized culture media obtained from 16HBE, exposed or not to CSE and/or pre-treated with NAC and FORM, was then undertaken. The two drugs are commonly used for the treatment of patients affected by chronic respiratory diseases (Dekhuijzen, 2004; Ferraro et al., 2017). NAC is a mucolytic drug while FORM is a long-acting beta 2 agonist. Here, these

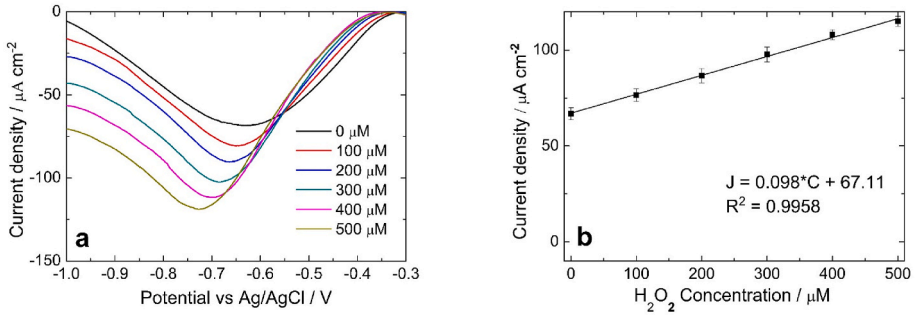

Fig. 5. a) LSV tests in the aerosol phase of MEM with different concentrations of H_2O_2. b) Corresponding calibration line with SD error bars (N = 3).

Table 1
Main features of the sensor.

Electrolyte	Sensitivity μA μM^{-1} cm^{-2}	Mean RSD	LOD μM
Liquid PBS	0.062 ± 0.0024	3.8%	60
Aerosol PBS	0.110 ± 0.0042	4%	30
Aerosol MEM	0.098 ± 0.0022	2%	40

two drugs were selected for their known antioxidant properties (Dekhuijzen, 2004; Ferraro et al., 2017). Fig. 6a presents typical LSVs obtained from different samples while Fig. 6b shows the mean concentrations of H_2O_2 calculated using the calibration line of Fig. 5b. CSE treatments led to an increase in H_2O_2 production while the treatment with the antioxidant NAC, and with the drug FORM caused its reduction.

To confirm that the results obtained using a sensor reflected an increase in intracellular oxidative stress, intracellular mitochondrial superoxide was evaluated using a ROS-sensitive fluorescent probe and flow cytometry, which is considered the gold standard for intracellular ROS quantification. After stimulation, cells were stained with Mitosox Red and analyzed by flow cytometry. The obtained results (Fig. 6c and Fig. S10) confirmed that CSE induced a significant increase of intracellular mitochondrial superoxide compared to non-treated cells (NT) and the pre-treatment with NAC and FORM reduced this effect. Thus, flow cytometry results paralleled those obtained with the sensor.

Finally, to evaluate the ability of the sensor to work in real operating conditions, samples of EBC were collected from a healthy subject and different known concentrations of H_2O_2 were then spiked into this and the LSV curves were recorded (Fig. 6d). The rationale of this experiment was to assess whether molecules present in EBC could interfere with the ability of the sensor to detect H_2O_2 altering its sensitivity. As it can be observed in Fig. 6d, the sensor can detect H_2O_2 in real breath matrices interferent-free.

Overall, these results suggest that the proposed sensor can be applied to the monitoring of cellular oxidative stress. Therefore, future applications may be foreseen for real-time monitoring of oxidative stress directly on patients by measuring the release of H_2O_2 in EB. This research sets the ground for the future development of novel systems for monitoring respiratory diseases based on the employment of a nanostructured sensor capable of quantifying H_2O_2 in EB. Thanks to its

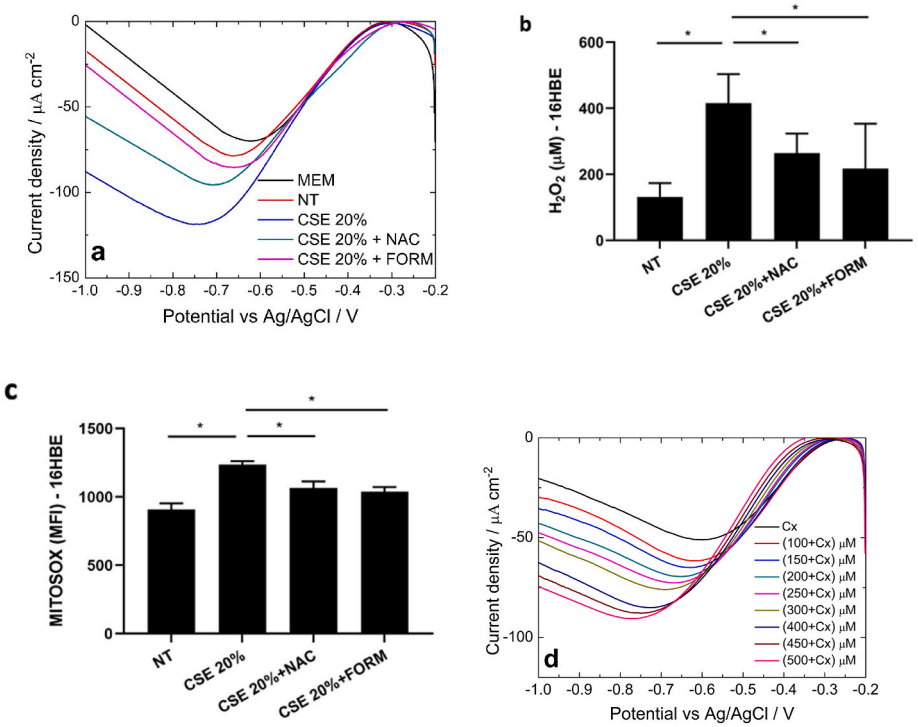

Fig. 6. a) LSV tests in the aerosol phase of nebulized culture media obtained from 16HBE. b) Mean concentration of H_2O_2 present in the samples (NT: non-treated cells; CSE: cells treated with cigarette smoke extract; CSE + NAC: cells treated with cigarette smoke extract and N-acetylcysteine; CSE + FORM: cells treated with cigarette smoke extract and Formoterol). N = 3 independent experiments. c) Mitochondrial superoxide production reported as Mean Fluorescence Intensity (MFI) ± SD (N = 3), *p < 0.05 Paired *t*-test, d) LSV tests in real EBC (Cx) before and after the addition of different amounts of hydrogen peroxide.

physical-chemical features, the proposed system, when integrated into a face mask for breath monitoring, will eliminate the condensation step required in the current clinical practice. The potential future applications of such an approach span a wide landscape of scenarios including homecare, remote point-of-care healthcare, and workplace diagnostics without the need for expensive laboratory equipment and skilled practitioners. The industrial relevance of this topic is confirmed by the market growth of low-cost wearable sensing devices generally reported by the most relevant market outlooks and forecasts currently available.

4. Conclusions

In this work, a low-cost and easy-to-use electrochemical sensor for the detection of hydrogen peroxide in exhaled breath was proposed. The proposed sensor was highly sustainable since the electrodes can be obtained from upcycling optical storage CD devices while an electrodeposited chitosan layer allows for the detection of hydrogen peroxide in the aerosol phase. A thorough optimization of electrodeposition process parameters (composition of the solution, deposition time, applied potential) was performed to obtain a uniform and homogenous film which is of paramount importance for the sensor to operate directly on the aerosol phase. Sensor performance was evaluated using LSV as the detection technique, with tests carried out using both liquid and aerosol phases. In both cases, the sensor returned a linear response in the range 100–500 μM with a sensitivity of 0.062 ± 0.0024 μA μM^{-1} cm^{-2} (RSD 3.8%) and a LOD of 60 μM in liquid PBS and a sensitivity of 0.110 ± 0.0042 μA μM^{-1} cm^{-2} (RSD 4%) and a LOD 30 μM in nebulized PBS. The sensors was also calibrated in MEM exhibiting a sensitivity of 0.098 ± 0.0022 μA μM^{-1} cm^{-2} (RSD 2%) and a LOD of 40 μM. The experimental results confirm that this sensor can operate in both liquid and aerosol phases without reduction in performance. The sensor had a very high selectivity as no interferences were observed. The sensor can quantify H_2O_2 in the aerosol phase released from human bronchial epithelial cells exposed to different pro-oxidant and antioxidant treatments. Of note, values obtained with this sensor was in line with those obtained using the conventional cytofluorimetric technique. Furthermore, the ability of the sensor to work with real EBC samples and after physical deformations has been successfully demonstrated.

Future research will focus on the optimization of the sensor fabrication process to overcome its limitations (i.e. to obtain stable external contacts and to increase the sensor sensitivity) and its industrial scale-up towards the miniaturization of the device. This would allow for the development of commercial solutions such as the integration into standard face masks for real-time monitoring of oxidative stress.

CRediT authorship contribution statement

M.G. Bruno: Writing – original draft, Methodology, Investigation. **B. Patella:** Writing – original draft, Validation, Methodology, Investigation. **M. Ferraro:** Writing – original draft, Validation, Formal analysis, Data curation. **S. Di Vincenzo:** Writing – original draft, Validation, Methodology, Investigation. **P. Pinto:** Formal analysis, Investigation. **C. Torino:** Supervision, Project administration, Funding acquisition. **A. Vilasi:** Formal analysis, Data curation. **M.R. Giuffrè:** Validation, Formal analysis, Data curation. **V.B. Juska:** Validation, Formal analysis, Data curation. **A. O'Riordan:** Writing – review & editing, Supervision, Conceptualization. **R. Inguanta:** Writing – review & editing, Writing – original draft, Supervision, Conceptualization. **C. Cipollina:** Writing – review & editing, Supervision, Conceptualization. **E. Pace:** Writing – review & editing, Supervision, Project administration, Funding acquisition, Conceptualization. **G. Aiello:** Writing – review & editing, Supervision, Project administration, Funding acquisition.

Declaration of competing interest

The authors declare that they have no known competing financial interests or personal relationships that could have appeared to influence the work reported in this paper.

Data availability

No data was used for the research described in the article.

Acknowledgments

This work was partially financed by: the project SENSOMAR (SEnsore Nanostrutturato per Stress Ossidativo integrato in MAscherina per valutazioni in Remoto MUR FISR 2020 IP_ 03106); the project "One Health Basic and Translational Research Actions addressing Unmet Needs on Emerging Infectious Diseases (IN-FACT) Proj n. PE00000007 CUP B53C20040570005; and a research grant from Science Foundation Ireland and the Department of Agriculture, Food and Marine on behalf of the Government of Ireland under the Grant 16/RC/3835 (VistaMilk).

Appendix A. Supplementary data

Supplementary data to this article can be found online at https://doi.org/10.1016/j.biosx.2024.100476.

References

Ainla, A., Mousavi, M.P.S., Tsaloglou, M.-N., Redston, J., Bell, J.G., Fernández-Abedul, M.T., Whitesides, G.M., 2018. Open-source potentiostat for wireless electrochemical detection with smartphones. Anal. Chem. 90, 6240–6246. https://doi.org/10.1021/acs.analchem.8b00850.

Altomare, L., Draghi, L., Chiesa, R., De Nardo, L., 2012. Morphology tuning of chitosan films via electrochemical deposition. Mater. Lett. 78, 18–21. https://doi.org/10.1016/j.matlet.2012.03.035.

Anh, D.T.V., Olthuis, W., Bergveld, P., 2005. A hydrogen peroxide sensor for exhaled breath measurement. Sensor. Actuator. B Chem. 111–112, 494–499. https://doi.org/10.1016/j.snb.2005.03.107.

Arodin Selenius, L., Wallenberg Lundgren, M., Jawad, R., Danielsson, O., Björnstedt, M., 2019. The cell culture medium affects growth, phenotype expression and the response to selenium cytotoxicity in A549 and HepG2 cells. Antioxidants 8, 130. https://doi.org/10.3390/antiox8050130.

Avcu, E., Baştan, F.E., Abdullah, H.Z., Rehman, M.A.U., Avcu, Y.Y., Boccaccini, A.R., 2019. Electrophoretic deposition of chitosan-based composite coatings for biomedical applications: a review. Prog. Mater. Sci. 103, 69–108. https://doi.org/10.1016/j.pmatsci.2019.01.001.

Aznar-Poveda, J., Lopez-Pastor, J., Garcia-Sanchez, A.-J., Garcia-Haro, J., Otero, T., 2018. A COTS-based portable system to conduct accurate substance concentration measurements. Sensors 18, 539. https://doi.org/10.3390/s18020539.

Baker, M., Assis, S., Higa, O., Costa, I., 2009. Nanocomposite hydroxyapatite formation on a Ti–13Nb–13Zr alloy exposed in a MEM cell culture medium and the effect of H2O2 addition. Acta Biomater. 5, 63–75. https://doi.org/10.1016/j.actbio.2008.08.008.

Besra, L., Liu, M., 2007. A review on fundamentals and applications of electrophoretic deposition (EPD). Prog. Mater. Sci. 52, 1–61. https://doi.org/10.1016/j.pmatsci.2006.07.001.

Bhide, A., Pali, M., Muthukumar, S., Prasad, S., 2022. EBC-SURE (exhaled breath condensate- scanning using rapid electro analytics): a non-faradaic and non-invasive electrochemical assay to screen for pro-inflammatory biomarkers in human breath condensate. Biosens. Bioelectron. 206, 114117 https://doi.org/10.1016/j.bios.2022.114117.

Boots, A.W., van Berkel, J.J.B.N., Dallinga, J.W., Smolinska, A., Wouters, E.F., van Schooten, F.J., 2012. The versatile use of exhaled volatile organic compounds in human health and disease. J. Breath Res. 6, 027108 https://doi.org/10.1088/1752-7155/6/2/027108.

Cai, X., Tanner, E.E.L., Lin, C., Ngamchuea, K., Foord, J.S., Compton, R.G., 2018a. The mechanism of electrochemical reduction of hydrogen peroxide on silver nanoparticles. Phys. Chem. Chem. Phys. 20, 1608–1614. https://doi.org/10.1039/C7CP07492A.

Cai, X., Tanner, E.E.L., Lin, C., Ngamchuea, K., Foord, J.S., Compton, R.G., 2018b. The mechanism of electrochemical reduction of hydrogen peroxide on silver nanoparticles. Phys. Chem. Chem. Phys. 20, 1608–1614. https://doi.org/10.1039/C7CP07492A.

Das, S., Pal, M., 2020. Review—non-invasive monitoring of human health by exhaled breath analysis: a comprehensive review. J. Electrochem. Soc. 167, 037562 https://doi.org/10.1149/1945-7111/ab67a6.

Davis, M.D., 2020. Exhaled breath condensate and aerosol. In: Breathborne Biomarkers and the Human Volatilome. Elsevier, pp. 109–119. https://doi.org/10.1016/B978-0-12-819967-1.00007-4.

Dekhuijzen, P.N., Aben, K.K., Dekker, I., Aarts, L.P., Wielders, P.L., van Herwaarden, C. L., Bast, A., 1996. Increased exhalation of hydrogen peroxide in patients with stable

and unstable chronic obstructive pulmonary disease. Am. J. Respir. Crit. Care Med. 154, 813–816. https://doi.org/10.1164/ajrccm.154.3.8810624.
Dekhuijzen, P.N.R., 2004. Antioxidant properties of N-acetylcysteine: their relevance in relation to chronic obstructive pulmonary disease. Eur. Respir. J. 23, 629–636. https://doi.org/10.1183/09031936.04.00016804.
Diouf, A., El Bari, N., Bouchikhi, B., 2020. A novel electrochemical sensor based on ion imprinted polymer and gold nanomaterials for nitrite ion analysis in exhaled breath condensate. Talanta 209, 120577. https://doi.org/10.1016/j.talanta.2019.120577.
Ferrari, A.C., 2007. Raman spectroscopy of graphene and graphite: disorder, electron–phonon coupling, doping and nonadiabatic effects. Solid State Commun. 143, 47–57. https://doi.org/10.1016/j.ssc.2007.03.052.
Ferraro, M., Gjomarkaj, M., Siena, L., Di Vincenzo, S., Pace, E., 2017. Formoterol and fluticasone propionate combination improves histone deacetylation and anti-inflammatory activities in bronchial epithelial cells exposed to cigarette smoke. Biochim. Biophys. Acta BBA - Mol. Basis Dis. 1863, 1718–1727. https://doi.org/10.1016/j.bbadis.2017.05.003.
Fiore, L., Mazzaracchio, V., Galloni, P., Sabuzi, F., Pezzola, S., Matteucci, G., Moscone, D., Arduini, F., 2021. A paper-based electrochemical sensor for H2O2 detection in aerosol phase: measure of H2O2 nebulized by a reconverted ultrasonic aroma diffuser as a case of study. Microchem. J. 166, 106249 https://doi.org/10.1016/j.microc.2021.106249.
Grob, N.M., Aytekin, M., Dweik, R.A., 2008. Biomarkers in exhaled breath condensate: a review of collection, processing and analysis. J. Breath Res. 2, 037004 https://doi.org/10.1088/1752-7155/2/3/037004.
Han, Z., Strycker, B.D., Commer, B., Wang, K., Shaw, B.D., Scully, M.O., Sokolov, A.V., 2020. Molecular origin of the Raman signal from Aspergillus nidulans conidia and observation of fluorescence vibrational structure at room temperature. Sci. Rep. 10, 5428. https://doi.org/10.1038/s41598-020-62112-w.
Inonu, H., Doruk, S., Sahin, S., Erkorkmaz, U., Celik, D., Celikel, S., Seyfikli, Z., 2012. Oxidative stress levels in exhaled breath condensate associated with COPD and smoking. Respir. Care 57, 413–419. https://doi.org/10.4187/respcare.01302.
Jiang, K., Back, S., Akey, A.J., Xia, C., Hu, Y., Liang, W., Schaak, D., Stavitski, E., Nørskov, J.K., Siahrostami, S., Wang, H., 2019. Highly selective oxygen reduction to hydrogen peroxide on transition metal single atom coordination. Nat. Commun. 10, 3997. https://doi.org/10.1038/s41467-019-11992-2.
Jiang, M., Wang, K., Kennedy, J.F., Nie, J., Yu, Q., Ma, G., 2010. Preparation and characterization of water-soluble chitosan derivative by Michael addition reaction. Int. J. Biol. Macromol. 47, 696–699. https://doi.org/10.1016/j.ijbiomac.2010.09.002.
Kaloumenou, M., Skotadis, E., Lagopati, N., Efstathopoulos, E., Tsoukalas, D., 2022. Breath analysis: a promising tool for disease diagnosis—the role of sensors. Sensors 22, 1238. https://doi.org/10.3390/s22031238.
Kaniyoor, A., Ramaprabhu, S., 2012. A Raman spectroscopic investigation of graphite oxide derived graphene. AIP Adv. 2, 032183 https://doi.org/10.1063/1.4756995.
Khalid, M.N., Agnely, F., Yagoubi, N., Grossiord, J.L., Couarraze, G., 2002. Water state characterization, swelling behavior, thermal and mechanical properties of chitosan based networks. Eur. J. Pharmaceut. Sci. 15, 425–432. https://doi.org/10.1016/S0928-0987(02)00029-5.
Kowalski, P., Łosiewicz, B., Goryczka, T., 2015. Deposition of chitosan layers on NiTi shape memory alloy. Arch. Metall. Mater. 60, 171–176. https://doi.org/10.1515/amm-2015-0027.
Lafuente, B., Downs, R.T., Yang, H., Stone, N., 2015. 1. The power of databases: the RRUFF project. In: Armbruster, T., Danisi, R.M. (Eds.), Highlights in Mineralogical Crystallography. DE GRUYTER, pp. 1–30. https://doi.org/10.1515/9783110417104-003.
Lin, T., Xu, Y., Zhao, A., He, W., Xiao, F., 2022. Flexible electrochemical sensors integrated with nanomaterials for in situ determination of small molecules in biological samples: a review. Anal. Chim. Acta 1207, 339461. https://doi.org/10.1016/j.aca.2022.339461.
Lopresti, F., Patella, B., Divita, V., Zanca, C., Botta, L., Radacsi, N., O'Riordan, A., Aiello, G., Kersaudy-Kerhoas, M., Inguanta, R., La Carrubba, V., 2022. Green and integrated wearable electrochemical sensor for chloride detection in sweat. Sensors 22, 8223. https://doi.org/10.3390/s22218223.
Lu, T., Ji, S., Jin, W., Yang, Q., Luo, Q., Ren, T.-L., 2023. Biocompatible and long-term monitoring strategies of wearable, ingestible and implantable biosensors: reform the next generation healthcare. Sensors 23, 2991. https://doi.org/10.3390/s23062991.
Maier, D., Laubender, E., Basavanna, A., Schumann, S., Güder, F., Urban, G.A., Dincer, C., 2019. Toward continuous monitoring of breath biochemistry: a paper-based wearable sensor for real-time hydrogen peroxide measurement in simulated breath. ACS Sens. 4, 2945–2951. https://doi.org/10.1021/acssensors.9b01403.
Manabe, S., Adavan Kiliyankil, V., Kumashiro, T., Takiguchi, S., Fugetsu, B., Sakata, I., 2020. Stabilization of Prussian blue using copper sulfate for eliminating radioactive cesium from a high pH solution and seawater. J. Hazard Mater. 386, 121979 https://doi.org/10.1016/j.jhazmat.2019.121979.
Murata, K., Fujimoto, K., Kitaguchi, Y., Horiuchi, T., Kubo, K., Honda, T., 2014. Hydrogen peroxide content and pH of expired breath condensate from patients with asthma and COPD. COPD 11, 81–87. https://doi.org/10.3109/15412555.2013.830094.
Nagaraja, C., Shashibhushan, B.Sagar, Asif, M., Manjunath, P., 2012. Hydrogen peroxide in exhaled breath condensate: a clinical study. Lung India 29, 123. https://doi.org/10.4103/0970-2113.95303.
Nobial, M., Devos, O., Mattos, O.R., Tribollet, B., 2007. The nitrate reduction process: a way for increasing interfacial pH. J. Electroanal. Chem. 600, 87–94. https://doi.org/10.1016/j.jelechem.2006.03.003.
O'Sullivan, B., O'Sullivan, S., Narayan, T., Shao, H., Patella, B., Seymour, I., Inguanta, R., O'Riordan, A., 2022. A direct comparison of 2D versus 3D diffusion analysis at nanowire electrodes: a finite element analysis and experimental study. Electrochim. Acta, 139890. https://doi.org/10.1016/j.electacta.2022.139890.
Patella, B., Aiello, G., Drago, G., Torino, C., Vilasi, A., O'Riordan, A., Inguanta, R., 2022a. Electrochemical detection of chloride ions using Ag-based electrodes obtained from compact disc. Anal. Chim. Acta 1190, 339215. https://doi.org/10.1016/j.aca.2021.339215.
Patella, B., Vincenzo, S.D., Zanca, C., Bollaci, L., Ferraro, M., Giuffrè, M.R., Cipollina, C., Bruno, M.G., Aiello, G., Russo, M., Inguanta, R., Pace, E., 2022b. Electrochemical quantification of H2O2 released by airway cells growing in different culture media. Micromachines 13, 1762. https://doi.org/10.3390/mi13101762.
Pleil, J.D., Wallace, M.A.G., Madden, M.C., 2018. Exhaled breath aerosol (EBA): the simplest non-invasive medium for public health and occupational exposure biomonitoring. J. Breath Res. 12, 027110 https://doi.org/10.1088/1752-7163/aa9855.
Połomska, J., Bar, K., Sozańska, B., 2021. Exhaled breath condensate—a non-invasive approach for diagnostic methods in asthma. J. Clin. Med. 10, 2697. https://doi.org/10.3390/jcm10122697.
Ren, X.D., Liu, Q.S., Feng, H., Yin, X.Y., 2014. The characterization of chitosan nanoparticles by Raman spectroscopy. Appl. Mech. Mater. 665, 367–370. https://doi.org/10.4028/www.scientific.net/AMM.665.367.
Rysz, J., Stolarek, R.A., Luczynski, R., Sarniak, A., Wlodarczyk, A., Kasielski, M., Nowak, D., 2007. Increased hydrogen peroxide concentration in the exhaled breath condensate of stable COPD patients after nebulized N-acetylcysteine. Pulm. Pharmacol. Ther. 20, 281–289. https://doi.org/10.1016/j.pupt.2006.03.011.
Shukla, S.D., Swaroop Vanka, K., Chavelier, A., Shastri, M.D., Tambuwala, M.M., Bakshi, H.A., Pabreja, K., Mahmood, M.Q., O'Toole, R.F., 2020. Chronic respiratory diseases: an introduction and need for novel drug delivery approaches. In: Targeting Chronic Inflammatory Lung Diseases Using Advanced Drug Delivery Systems. Elsevier, pp. 1–31. https://doi.org/10.1016/B978-0-12-820658-4.00001-7.
Szunerits, S., Dörfler, H., Pagneux, Q., Daniel, J., Wadekar, S., Woitrain, E., Ladage, D., Montaigne, D., Boukherroub, R., 2023. Exhaled breath condensate as bioanalyte: from collection considerations to biomarker sensing. Anal. Bioanal. Chem. 415, 27–34. https://doi.org/10.1007/s00216-022-04433-5.
Tiele, A., Wicaksono, A., Ayyala, S.K., Covington, J.A., 2020. Development of a compact, IoT-enabled electronic nose for breath analysis. Electronics 9, 84. https://doi.org/10.3390/electronics9010084.
Toniolo, R., Geatti, P., Bontempelli, G., Schiavon, G., 2001. Amperometric monitoring of hydrogen peroxide in workplace atmospheres by electrodes supported on ion-exchange membranes. J. Electroanal. Chem. 514, 123–128. https://doi.org/10.1016/S0022-0728(01)00612-X.
Tran, Hoang V., Huynh, C.D., Tran, Hanh V., Piro, B., 2018. Cyclic voltammetry, square wave voltammetry, electrochemical impedance spectroscopy and colorimetric method for hydrogen peroxide detection based on chitosan/silver nanocomposite. Arab. J. Chem. 11, 453–459. https://doi.org/10.1016/j.arabjc.2016.08.007.
Wang, S., Yu, P., Li, Xinjin, Zhao, Z., Dong, Y., Li, Xiangye, 2023. Design and fabrication of functional hydrogels with specific surface wettability. Colloid Interface Sci. Commun. 52, 100697 https://doi.org/10.1016/j.colcom.2023.100697.
Wang, Z., Yang, H., Gao, B., Tong, Y., Zhang, X., Su, L., 2014. Stability improvement of Prussian blue in nonacidic solutions via an electrochemical post-treatment method and the shape evolution of Prussian blue from nanospheres to nanocubes. The Analyst 139, 1127. https://doi.org/10.1039/c3an02071a.